Explosion induced domino effect assessment in the process industries

A machine learning approach to improve probit models

Jiang, Min; Yang, Yu; Bian, Jiexiang; Fang, Mengru; Cozzani, Valerio; Reniers, Genserik; Chen, Chao

DOI
10.1016/j.jlp.2025.105714

Publication date
2025

Document Version
Final published version

Published in
Journal of Loss Prevention in the Process Industries

Journal of Loss Prevention in the Process Industries 98 (2025) 105714

Contents lists available at ScienceDirect

Journal of Loss Prevention in the Process Industries

journal homepage: www.elsevier.com/locate/jlp

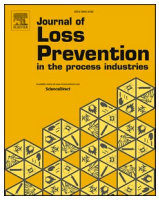

Explosion induced domino effect assessment in the process industries: A machine learning approach to improve probit models

Min Jiang [a], Yu Yang [b], Jiexiang Bian [b], Mengru Fang [a], Valerio Cozzani [c], Genserik Reniers [d], Chao Chen [a,*]

[a] Petroleum Engineering School, Southwest Petroleum University, Chengdu, China
[b] School of Mechanical Engineering, Southwest Petroleum University, Chengdu, 610500, China
[c] LISES— Laboratory of Industrial Safety and Environmental Sustainability, DICAM, University of Bologna, Bologna, 40126, Italy
[d] Faculty of Technology, Policy and Management, Safety and Security Science Group (S3G), TU Delft, 2628 BX, Delft, the Netherlands

ARTICLE INFO

Keywords:
Domino effect
Overpressure
Blast wave
Machine learning
Quantitative risk assessment
Chemical process industry

ABSTRACT

Explosion-induced domino accidents in the chemical industry, such as the 2005 Buncefield and 2019 Xiangshui accidents, can lead to catastrophic losses. Recent studies commonly use probit models (simplified linear regression models) to predict the probability of accident escalation caused by equipment failure due to overpressure conditions but necessitate distinct equations for different equipment types. In order to simplify the number of models and improve their accuracy, this study introduced three machine learning models (random forest model, convolutional neural network model, and deep neural network model), addressing complex nonlinear relationships that conventional regression models may not fully capture. By model training, the DNN model has the highest accuracy (99 %), followed by CNN (94 %) and random RF (95 %). The DNN model was selected as the optimal data-driven model for equipment vulnerability assessment due to their feedforward mechanism's capability to dynamically align parameters with evolving data distributions. The approach developed can not only predict the probability of equipment damage by integrating values related to peak overpressure and equipment type but also effectively address the accuracy validation issues associated with traditional regression models. Besides, this approach can be considered open source model and more explosion data may be used in the future to further improve the model.

1. Introduction

The past few decades have witnessed a substantial escalation in the manufacturing of chemicals within emerging economies due to the massive transformations of worldwide economic structure (Wang et al., 2021). Amidst the remarkable development of chemical industry, many chemical industrial parks (CIP) have been established worldwide (Zeng et al., 2024). Although these industrial clusters deliver significant industrial efficiency, the increase in the risk of major accidents caused by dangerous substances cannot be ignored (Casciano et al., 2019). Clearly, a primary accident (e.g., fire and explosion) may escalate to nearby equipment, triggering a sequence of accidents, resulting in overall consequences more severe than those of the primary scenario, which is called "domino effect" (Reniers and Cozzani, 2013a). The term derived from the game of domino toppling involves rectangular pieces made of wood or plastic in which players arrange the dominoes in a linear formation at specified intervals and gently knock over the first piece, causing the adjacent dominoes to fall sequentially (Khan and Abbasi, 2001). In terms of domino effect accidents in CIP, they can be triggered by blast waves, fire, fragment projection, or a combination of the above (Salzano and Cozzani, 2004b). Thus, a domino effect accident can generate serious consequences (Reniers et al., 2005). For instance, on October 23, 2009, a tank overflow at the Caribbean Petroleum Company (CAPECO) in Bayamon, Puerto Rico, led to an explosion. This incident caused 3 injuries and severely damaged 48 storage tanks, affecting 300 business and residential buildings within a 2-km radius (CBS, 2015). On March 21, 2019, the massive explosion in Tianjiayi Chemical Co., Ltd., Xiangshui CIP, China, resulted in 78 deaths, more than 640 injuries, economic losses of 19.86 billion CNY, affecting 16 chemical plants in the adjacent area (Zhang et al., 2019). The initial incident was an explosion

This article is part of a special issue entitled: Explosion Safety published in Journal of Loss Prevention in the Process Industries.

* Corresponding author.
E-mail address: chenchaoswpu@gmail.com (C. Chen).

https://doi.org/10.1016/j.jlp.2025.105714
Received 25 February 2025; Received in revised form 5 June 2025; Accepted 15 June 2025
Available online 17 June 2025

of solid waste and the generated blast wave and debris triggered escalation scenarios resulting in a domino effect (Yang et al., 2020). On May 1, 2023, an explosion and fire occurred at the sodium percarbonate production area of Luxi Chemical in Liaochen, China, resulting in 9 deaths, 1 injury, 1 missing (Xinhua, 2023a). On November 29, 2023, a fire at a chemical factory in India's western state of Gujarat, injured 24 workers (Xinhua, 2023b). On July 26, 2024, an explosion at a factory in an industrial park of Yongcheng city in China's Henan province, killed 5 people and slightly injured 14 others (Xinhua, 2024).

In order to manage control and mitigate the risk associated with domino accident scenarios, many researchers have investigated the quantitative risk assessment of domino effects. One of the key factors in domino effect assessment is the development of an accurate vulnerability model of equipment exposed to fire and explosion. Cozzani et al. provided an approach for the quantitative risk assessment (QRA) of domino effect based simplified equipment damage models suitable for the application in a QRA framework(Cozzani et al., 2005). Reniers et al. and Cozzani et al. consolidated established the current framework for the assessment of domino effect, recognizing the availability of improved equipment fragility models as a key enabling factor for the assessment of domino effect(Cozzani and Reniers, 2021; Reniers and Cozzani, 2013b). Cozzani et al. proposed escalation thresholds derived from modeling the damage to process equipment caused by heat radiation, overpressure, and fragment projection due to fire (Cozzani et al., 2006). Landucci et al. employed a multi-level approach to analyze the failure of vessel walls under various fire conditions, resulting in a simplified model that correlates the time to failure (ttf) of the vessel with the radiation intensity of its shell, aiming to quantitatively assess the risk from fire-triggered escalation scenarios (Landucci et al., 2009). Building upon the recent definition of the domino effect, as well as the established escalation threshold and safe distance, Alileche et al. conducted a comprehensive physical analysis of the escalation mechanism and developed procedures to identify the most suitable values (Alileche et al., 2015). Chen et al. developed a dynamic graph method to simulate the spatial-temporal evolution of the domino accidents, thereby effectively circumventing the limitations inherent in the "probit model" for the estimation of fire propagation probabilities (Chen et al., 2018). Yang et al. developed a quantitative model based on the failure time of atmospheric storage tanks under coupled pool fires, enabling direct calculation of the failure time for storage tanks subjected to multi-pool fire coupling and offering recommendations for mitigating the domino effect (Yang et al., 2023). Based on the ability of fire dynamics simulator (FDS) fluid code to detect random flame movement at any time, Pourkeramat et al. employed a fire dynamics simulator FDS to assess pool fire radiation and soot concentration (Pourkeramat et al., 2021). Building upon this foundation, Malik et al. employed artificial neural network (ANN) based on numerical dataset to predict the probability of fire spread(Malik et al., 2023).

Compared to fire accidents, research on escalation caused by blast waves is relatively scarce. Predictions of equipment damage caused by blast waves primarily relies on probit models. Eisenberg et al. first introduced a probit model to establish a function between overpressure and its detrimental impact on equipment:

$$Y = -23.8 + 29.2\ln(\Delta P) \tag{1}$$

Where Y is probit value, ΔP is overpressure (Eisenberg et al., 1975). Based on data concerning equipment damage in explosion scenarios, Cozzani et al. divided the equipment into four categories and obtained specific fragility models based on probit equations, significantly improving the performance of the correlation with respect to the model of Eisenberg et al., even if the MSE of the probit function was still more than 40 percent (Cozzani and Salzano, 2004). Zhang and Jiang et al. adopted Cozzani's methodology to categorize the equipment into four distinct classifications and revised the damage grading standards further enhancing the accuracy of the probit functions(Zhang and Jiang, 2008). Mukhim et al. introduced a further categorization of equipment, dividing process equipment in 13 categories, improving to some extent the accuracy of the model (Mukhim et al., 2017a). Thus, scholars have gradually upgraded the existing models to assess blast wave damage induced by domino effects, but the accuracy of such models is still limited, also due to the non-homogeneous nature of the scarce data concerning equipment damage caused by blast waves available in the open literature.

Currently, machine learning is extremely popular and has been applied with success to develop data-driven models in various fields. Roxas II et al. combined machine learning with visual flow regime to predict flow patterns in pipelines in process industries (Roxas II et al., 2022). Hamid et al. developed a machine learning model utilizing multiple regression techniques and data generated from process simulation models. This model was successfully implemented in a gas processing plants in Malaysia (Hamid et al., 2022). In order to consider the response of equipment to hazardous loads, Lan et al. extended a hazardous scenario module at the front end of the domino effect assessment framework and developed a network-based approach to simulate the domino effect related to natural disasters (Lan et al., 2022). Jablonka et al. exploited a machine learning model to predict the amine emissions of carbon capture devices and simulated the impacts of interventions, making contribution to optimize the operation of power plants, reducing noxious gas emissions, and improving the safety of chemical processes (Jablonka et al., 2023). Zhao et al. proposed a hybrid neural network combined with fault threshold optimization algorithm for online temperature prediction and anomaly diagnosis in lithium batteries (Zhao et al., 2024). Tian et al. introduced a graph neural network-based Design for Manufacturability (DFM) search algorithm This algorithm can adaptively pinpoint image samples that epitomize DFM through the process of image classification, facilitating the recognition of DFM, and circumventing the issue of combinatorial explosion that may emerge during the search process (Tian et al., 2024). Zhang et al. integrated the probability failure mechanism of power flow distribution and components to accurately describe the dynamic cascading failure process. This model utilized deep reinforcement learning to generate real-time remedial measures, alleviating cascading failures in the power grid (Zhang et al., 2024). Zhu et al. combined convolutional neural networks and transformer networks to construct a single station deep learning network architecture, proposed a high-speed railway earthquake early warning (EEW) method using deep learning (Zhu et al., 2024). Li et al. presented a novel Trusted Mechanical Fault Diagnosis (TMFD) method that integrates Bayesian deep learning techniques with model calibration strategies. Meng et al. used data-driven Bayesian networks for risk analysis, providing theoretical basis for risk prevention and control of lithium-ion battery and oil spill collection system accidents (Meng et al., 2024, 2025).The effectiveness and robustness of this approach were demonstrated through experimental datasets in mechanical fault diagnosis (Li et al., 2025). Xing et al., based on deep neural network models, proposed two dynamic response models for single arm high-rise buildings subjected to geological hazards (Xing et al., 2025).

Nevertheless, machine learning had never been applied to the quantitative assessment of escalation, and in particular to the analysis of equipment damage due to blast waves in order to obtain the probability of escalation. Critical factors governing chemical processing equipment explosion dynamics include: peak overpressure, blast waves duration, target distance, and equipment specifications (Men et al., 2021). Relevant research indicates that the destructive effects of a gas explosion stem primarily from the high-pressure of the shock wave (Wang et al., 2017). Peak overpressure serves as a critical parameter for assessing equipment damage severity, with its magnitude directly influencing the probability of accident escalation (Landucci et al., 2009). In the present study, an existing probit model has been enhanced by machine learning techniques to quantify the probability of explosion-induced accident escalation under varying overpressure values and equipment types. This approach dramatically improves the accuracy of probit model while

Table 1
Literature data available reporting damage probability to process equipment by peak overpressure caused by the blast waves.

ΔP_{max}(kPa)	Damage	Probability(%)	Reference
3.5	Louvers fall at 0.2–0.5 psi	10.00	CCPS (1999)
5.2	Minor damage, cone roof tank (100 % filled)	10.00	Mukhim et al. (2017a)
5.2	Minor damage, cone roof tank (50 % filled)	10.00	Mukhim et al. (2017a)
6.9	Collapse of cone tank roof	50.00	CCPS (1999)
7.0	Collapse of atmospheric tank roof	10.00	Zhang and Jiang (2008)
10.0	50 % damage to atmospheric tank	50.00	Mukhim et al. (2017a)
10.0	Failure of atmospheric equipment	65.00	Mukhim et al. (2017a)
10.3	Cooling towers connection failures	40.00	Mukhim et al. (2017a)
13.8	Cooling towers support structure damage	50.00	CCPS (1999)
13.8	Windows and gauges broken	5.45	CCPS (1999)
13.8	Debris-missile damage occurs	10.00	CCPS (1999)
17.0	Minor damage, distillation tower and cylindrical steel vertical structures	10.00	Mukhim et al. (2017a)
18.7	Catastrophic failure, cone roof tank	94.40	Mukhim et al. (2017a)
18.7	Minor damage, reactor cracking	10.00	Mukhim et al. (2017a)
18.7	Minor damage, floating roof tank (50 % filled)	10.00	Mukhim et al. (2017a)
20.0	Deformation of atmospheric tank	90.00	Mukhim et al. (2017a)
20.0	100 % damage, atmospheric tank	98.00	Mukhim et al. (2017a)
20.7	Floating roof atmospheric pressure vessels half tilted	29.46	CCPS (1999)
21.0	Destruction of fixed roof atmospheric tank	98.40	Zhang and Jiang (2008)
24.0	20 % damage of steel floating roof tank	32.58	Mukhim et al. (2017a)
24.1	Cooling towers frame collapse	90.00	CCPS (1999)
24.1	Reactors used for cracking operations moves and pipes break	30.00	CCPS (1999)
25.0	Atmospheric tank destruction	100.00	Mukhim et al. (2017a)
25.3	Minor damage, reactor chemical	10.00	Mukhim et al. (2017a)
27.6	Chemical reactors moves and pipes break	34.62	CCPS (1999)
31.0	Filter damaged	50.00	CCPS (1999)
35.0	Damage of fractionating column	50.00	Zhang and Jiang (2008)
37.9	Frame cracks, fractionation column	90.00	CCPS (1999)
39.1	Minor damage, pressure vessel horizontal	10.00	Mukhim et al. (2017a)
41.4	Horizontal pressurized vessels moves and pipe breaks	50.00	CCPS (1999)
42.5	Cone roof tank (100 % filled)	100.00	Mukhim et al. (2017a)
42.5	Minor damage, floating roof tank (100 % filled)	50.00	Mukhim et al. (2017a)
42.5	Minor damage, extraction column	10.00	Mukhim et al. (2017a)
44.8	Chemical reactors moves and pipes break	50.00	CCPS (1999)
44.8	Unit moves and pipe breaks, extraction column	50.00	CCPS (1999)
44.8	Unit uplifts (0.9 tilted)	90.00	CCPS (1999)
45.0	Catastrophic failure, floating roof tank	93.26	Zhang and Jiang (2008)
45.9	Catastrophic failure, fraction column	99.51	Mukhim et al. (2017a)
48.3	Fractionating column overturns or destroyed	100.00	CCPS (1999)
48.3	Reactors used for cracking operations moves and pipes break	50.00	CCPS (1999)
49.3	Minor damage, heat exchanger	10.00	Mukhim et al. (2017a)
51.7	Heat exchangers moves and pipes break	50.00	CCPS (1999)
52.7	Minor damage, tank sphere	10.00	Mukhim et al. (2017a)
55.0	20 % structural damage of spherical steel petroleum tank	49.88	Mukhim et al. (2017a)
55.2	Pressure vessel spherical moves and pipe breaks	50.00	CCPS (1999)
59.5	Catastrophic failure, reactor chemical	99.59	Mukhim et al. (2017a)
59.5	Catastrophic failure, heat exchanger	99.59	Mukhim et al. (2017a)
61.2	Catastrophic failure, pressure vessel horizontal	99.87	Mukhim et al. (2017a)
62.1	Chemical reactors overturn or is destroyed	100.00	CCPS (1999)
62.1	Pressure vessel horizontal overturns or is destroyed	100.00	(CCPS, 1999))
62.1	Heat exchangers overturn or is destroyed	100.00	CCPS (1999)
65.5	Filtration moves on foundation	90.00	CCPS (1999)
69.0	Extraction columns moves on foundation	90.00	CCPS (1999)
69.7	Catastrophic failure, extraction column	98.43	Mukhim et al. (2017a)
70.0	Failure of pressurized storage sphere	90.00	Zhang and Jiang (2008)
76.5	Catastrophic failure, reactor cracking	99.14	Mukhim et al. (2017a)
81.6	Minor damage, pressure vessel vertical	10.00	Mukhim et al. (2017a)
82.7	Extraction columns overturn or is destroyed	100.00	CCPS (1999)
82.7	Filtration overturns or destroyed	100.00	CCPS (1999)
82.7	Pressure vessel vertical moves and pipe breaks,	49.87	CCPS (1999)
83.0	20 % damage of vertical cylindrical steel pressure	50.00	Mukhim et al. (2017a)
83.7	Reactors used for cracking operations overturn or is destroyed	100.00	CCPS (1999)
88.4	Catastrophic failure, pressure vessel vertical	99.12	Mukhim et al. (2017a)
95.3	99 % structural damage of vertical, steel pressure vessel	99.82	Mukhim et al. (2017a)
96.5	Pressure vessel vertical destroyed	99.95	CCPS (1999)
97.0	99 % damage of vertical cylindrical steel pressure vessel	100.00	Mukhim et al. (2017a)
108.8	Catastrophic failure, tank sphere	99.86	Mukhim et al. (2017a)
108.9	99 % structural damage of spherical pressure steel vessel	99.87	Mukhim et al. (2017a)
110.0	99 % damage of spherical steel petroleum tank	99.97	Mukhim et al. (2017a)
110.3	Pressure vessel spherical destroyed	100.00	CCPS (1999)
136.1	Floating roof tank (50 % filled)	99.86	Mukhim et al. (2017a)
136.1	Floating roof tank (100 % filled)	99.86	Mukhim et al. (2017a)
136.1	99 % structural damage of floating roof tank	99.87	Mukhim et al. (2017a)
137.1	99 % damage of floating roof petroleum tank	99.93	Mukhim et al. (2017a)
137.9	Collapse of floating tank roof	100.00	CCPS (1999)

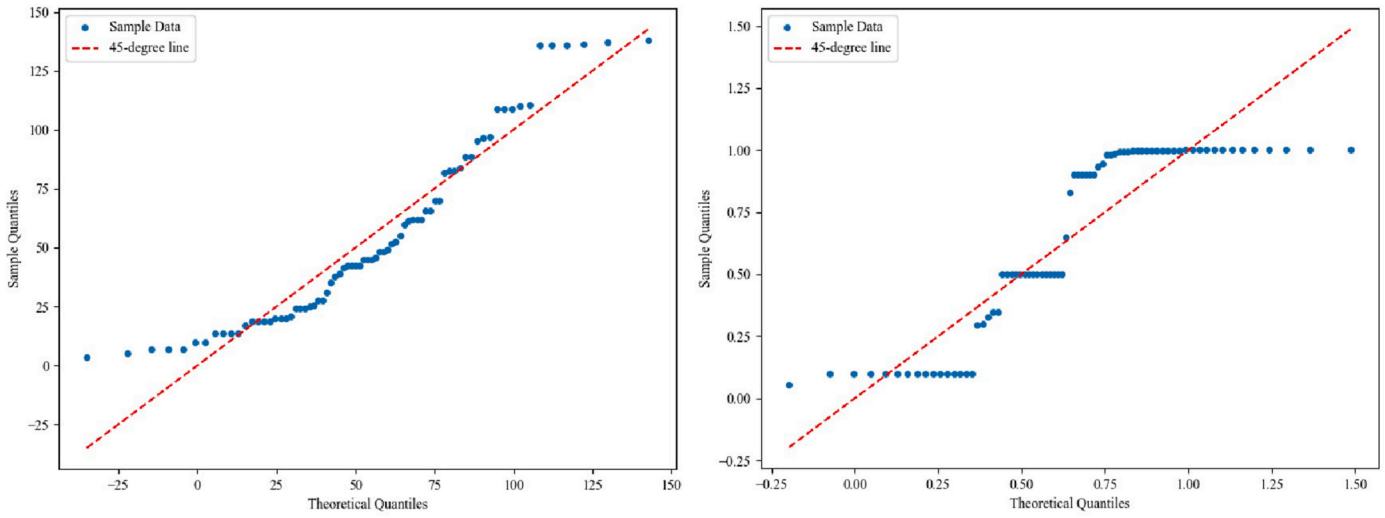

Fig. 1. Probability-probability Plot.

computational requirements in the application of the models.

2. Equipment damage data caused by overpressure

Experimental studies addressing the damage induced by blast waves are scarce. Consequently, correlations addressing damage probability with respect to the intensity of the blast wave generated by the explosion must be assessed primarily based on data derived from historical accident analyses and the limited existing experimental findings. Such data often encompass only qualitative descriptions of the observed extent of damage resulting from specific levels of peak overpressure. The dataset utilized in this article originates from the analysis and systematic revision of data published in the open literature and is presented in Table 1 (CCPS, 1999; Cozzani and Salzano, 2004; Mukhim et al., 2017a; Zhang and Jiang, 2008).

Accurately assessing the risk of domino effects hinges on two critical factors: quantifying the likelihood that an initial event will trigger subsequent, more severe incidents, and evaluating the extent of equipment and structural damage by analyzing the relationship between overpressure and its effects(Mukhim et al., 2017a). In industrial settings, overpressure levels are generally found to be strongly and positively correlated with the severity of structural damage. To estimate the associated probabilities, Mukhim et.al. proposed the following equation, which can connect the overpressure value and the probability value:

L: Minimum loss or damage (probability range 0–10 %);
M:Moderate loss or damage (probability range 10–50 %);
S:Serious loss or damage (probability range 50–90 %);
C:Catastrophic loss or damage (probability range 90–100 %);

$$P=\begin{cases}0.1\left(\dfrac{\Delta P}{\Delta P_{\max}}\right)\times 100 & \text{L}\\ \left\{0.4\left(\dfrac{\Delta P}{\Delta P_{\max}}\right)+0.1\right\}\times 100 & \text{M}\\ \left\{0.5\left(\dfrac{\Delta P}{\Delta P_{\max}}\right)+0.4\right\}\times 100 & \text{S}\\ \left\{0.1\left(\dfrac{\Delta P}{\Delta P_{\max}}\right)+0.9\right\}\times 100 & \text{C}\end{cases} \tag{2}$$

The data from previous accidents were subjected to a normality test concerning the overpressure values and probability values, with the results illustrated in Fig. 1. Under a normal distribution, the cumulative distribution function (CDF) values of the sample data should correspond

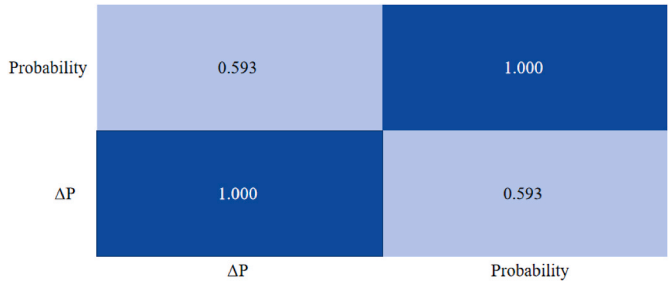

Fig. 2. Correlation heatmap.

to those of the standard normal distribution. If the sample data adheres to a normal distribution, then points on the Probability-Probability Plot would approximate a diagonal line. However, it is evident that the probability value in Fig. 1 do not conform to a normal distribution.

Given that the data do not meet the assumption of normality, Spearman's rank correlation coefficient is selected to assess correlations within the dataset. Spearman correlation analysis is a statistical method employed to quantify the degree of association between ordered variables, with results primarily expressed through the significance level (P-value) and correlation coefficient (R-value). The computation of Spearman's rank correlation coefficient is:

$$\rho=\frac{\sum_{i=1}^{n}(x_i-\overline{x})(y_i-\overline{y})}{\sqrt{\sum_{i=1}^{n}(x_i-\overline{x})^2\sum_{i=1}^{n}(y_i-\overline{y})^2}} \tag{3}$$

Where, ρ is the significance level, x_i is the rank of x, the y_i is the rank of y.

The results indicate that the P-value associated with ΔP value and probability value is less than 0.001 (corresponding to a significance level of 1 %), suggesting that at a confidence level of 99.9 %, the observed correlation is unlikely attributable to random chance but rather possesses substantive significance. Moreover, the correlation coefficient between ΔP value and probability value is 0.593, indicating a positive linear relationship. Specifically, as one variable increases, there is a tendency for the other variable to increase as well, although the correlation is not sufficiently strong. The specific correlation heatmap is shown in Fig. 2.

Due to the lack of a sufficient linear correlation between

Table 2
Probability value caused by blast waves for various equipment.

Equipment type	ΔP_{max}(kPa)	Probability (%)
vertical pressurized vessels	81.6	10
	82.7	49.87
	83	50
	88.4	99.12
	95.3	99.82
	96.5	99.95
	97	100
other atmospheric pressure vessels	7	10
	7	10
	10	50
	10	65
	20	90
	20	98
	21	98.4
	25	100
extraction columns	42.5	10
	44.8	50
	69	90
	69.7	98.43
	82.7	100
conical roof atmospheric pressure vessels	5.2	10
	5.2	10
	6.9	50
	18.7	94.4
	42.5	100
filtration units	13.79	10
	31.03	50
	65.5	90
	82.74	100
fractionating column/distillation towers	17	10
	35	50
	37.9	90
	45.9	99.51
	48.3	100
reactors used for cracking operations	18.7	10
	24.1	30
	48.3	50
	76.5	99.14
	83.7	100
other chemical reactors	13.8	5.45
	25.3	10
	27.6	34.62
	44.8	50
	59.5	99.59
	62.1	100
horizontal pressurized vessels	39.1	10
	41.4	50
	61.2	99.87
	62.1	100
heat exchangers	49.3	10
	51.7	50
	59.5	99.59
	62.1	100
cooling towers	3.45	10
	10.34	40
	13.79	50
	24.13	90
spherical pressurized vessels	52.7	10
	55	49.88
	55.2	50
	70	90
	108.8	99.86
	108.9	99.87
	110	99.97
	110.3	100
floating roof atmospheric pressure vessels	18.7	10
	20.7	29.46
	24	32.58
	42.5	50
	44.8	90
	45	93.26
	136.1	99.86
	136.1	99.86
	136.1	99.87
	137	99.93
	137.9	100

overpressure values and probability values, traditional probability models often struggle with nonlinear data because they assume fixed, linear relationships between variables. This makes them unsuitable for capturing complex behaviors such as interactions between multiple factors. Such limitations are especially critical when modeling domino effect risks, where damage often escalates in nonlinear ways. In contrast, machine learning models can flexibly learn these patterns without predefined assumptions. Therefore, we adopted a data-driven approach to better handle the nonlinear characteristics in our dataset.

The equipment has been divided into 13 categories (horizontal pressurized vessels, spherical pressurized vessels, vertical pressurized vessels, conical roof atmospheric pressure vessels, floating roof atmospheric pressure vessels, other atmospheric pressure vessels, cooling towers, fractionation columns, extraction columns, reactors used for cracking, other chemical reactors, heat exchangers and filtration unit) as in the previous study by Mukhim et al. The available data for blast wave damage was then divided considering the 13 categories of equipment introduced in the study. Table 2 shows the data pertaining to each of the categories.

Considering the substantial variations in vulnerability among diverse types of equipment, the inclusion of equipment type as a highly correlated feature within the model furnishes information intimately tied to the target variable. This incorporation is anticipated to substantially elevate both the precision and dependability of the model's predictive capabilities.

3. Method

The approach developed first arranges historical data and classifies the equipment involved in each accident, and then establishes three machine learning models (the random forest model, the convolutional neural network model and the deep neural network model). Machine learning methods were used to study the correlations between equipment damage and blast wave intensities, that are crucial in the risk assessment of the domino effect induced by overpressure in chemical processes. Dynamic physical parameters including blast source distance and shock wave duration are largely unavailable due to incomplete field records. However, more detailed categorization (incorporating size and storage media) leads to reduced data volume per category, which may negatively impact model fitting. For instance, in skin cancer classification tasks, models perform excellently in coarse-grained classification (benign vs. malignant) but require the use of transfer learning and data augmentation to compensate for insufficient data when subdivided into 20+ cancer subtypes (Esteva et al., 2017). Consequently, we prioritized equipment type (classified into thirteen distinct types) and overpressure values as key input features, a methodology robustly validated in prior studies for quantifying initial escalation risks via static vulnerability curves (Cozzani and Salzano, 2004; Landucci et al., 2009; Mukhim et al., 2017b; Salzano and Cozzani, 2004a; Zhang and Jiang, 2008). Finally, by employing the trained prediction model the corresponding probability value for damage is obtained. In general, a common empirical standard for dividing machine learning datasets is 70 % for the training set and 30 % for the testing set, this ratio can be adjusted with the size of the dataset and the number of feature values. For example, in research on predicting the accidental release of toxic chemicals, Hassan et al. used 80 % of the simulated data to train the ML model (Hassan et al., 2025). Cho et al. trained a machine learning model to predict the location of the leak source, and the training and testing datasets were randomly divided into a ratio of 7:3 (Cho et al., 2018). Nie et al. employed Residual Neural Networks (ResNet) and Artificial Neural Networks (ANN) to predict the critical quench thickness of combustible gas in pipelines,with the dataset partitioned into training and testing sets at a 4:1 ratio (Nie et al., 2024). However, due to the small volume of available data in this study, we adopted a ratio of 5:1 for the training set to the testing set. This approach was necessary to maximize the use of available data for training the model. Furthermore, to ensure the prediction performance is

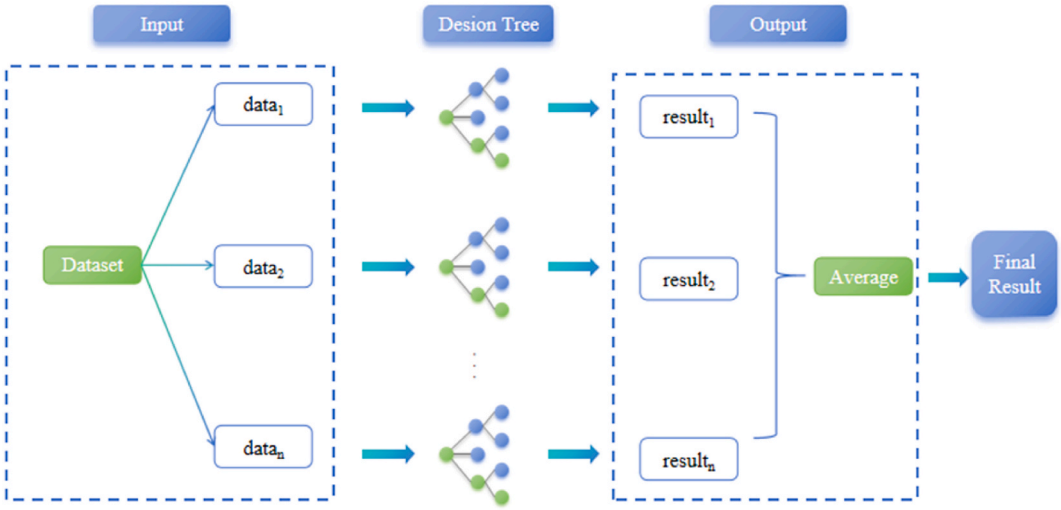

Fig. 3. The schematic diagram of the Random Forest model.

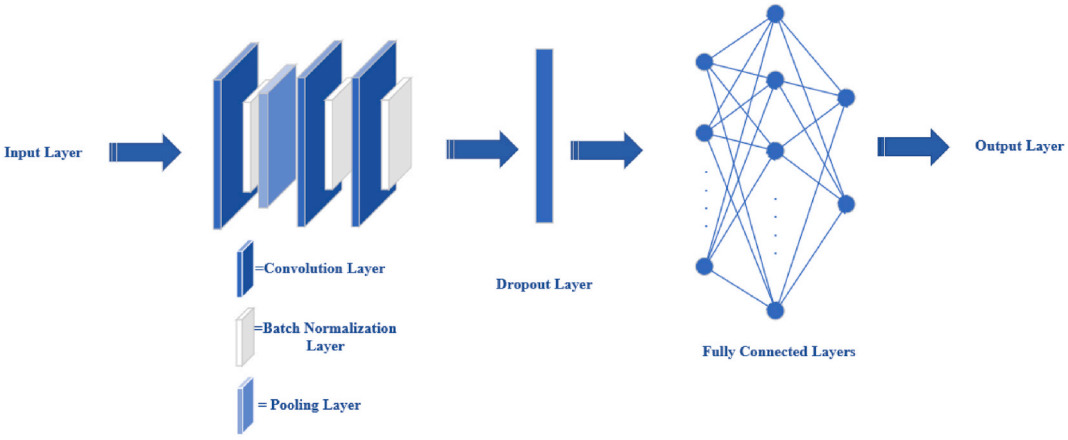

Fig. 4. The schematic diagram of the Convolutional Neural Network model.

representative for all equipment types, we ensured that the test set includes data from all equipment categories when partitioning the data. This way, the model's accuracy is tested across the full range of equipment types.

3.1. Random forest model

The random forest model, proposed in 2001, is an ensemble learning method that employs voting among multiple decision trees to arrive at final predictions (Biau and Scornet, 2016). This integrated learning strategy mitigates the risk of overfitting. Each decision tree is trained on a distinct subset of data, which introduces randomness and consequently reduces the model's excessive dependence on the training dataset. While this approach preserves high levels of accuracy and generalization.

This random forest model employs GridSearchCV for hyperparameter tuning, systematically exploring various parameter combinations through grid search. A 5-fold cross-validation approach is utilized to assess the performance of each parameter combination, thereby ensuring the model's stability and generalization capability. The model presented in this article is illustrated in Fig. 3.

3.2. Convolutional neural network model

Convolutional neural network model effectively process data through local perception and parameter sharing. This model optimizes network weights via the backpropagation algorithm, which is particularly beneficial in minimizing overfitting when working with limited data, aiming to minimize the loss function. The model is illustrated in Fig. 4.

The Adam algorithm is used to adjust the learning rate of each parameter by calculating the first-order momentum (exponentially weighted average of gradients) and second-order momentum (exponentially weighted average of squared gradients). The specific formula is as follows.

1. The first-order momentum:

$$m_t = \beta_1 m_{t-1} + (1-\beta_1) g_t \tag{4}$$

2. The second-order momentum:

$$v_t = \beta_2 v_{t-1} + (1-\beta_2) g_t^2 \tag{5}$$

3. Deviation correction:

$$\widehat{m}_t = \frac{m_t}{1-\beta_1^t} \tag{6}$$

$$\widehat{v}_t = \frac{v_t}{1-\beta_2^t} \tag{7}$$

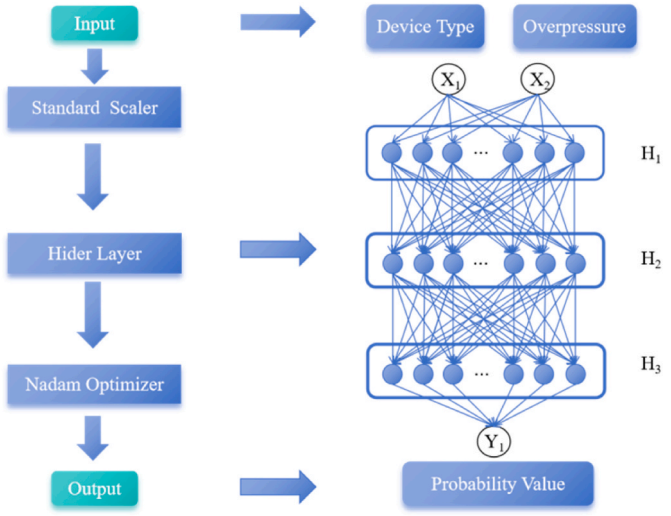

Fig. 5. The schematic diagram of the Deep Neural Network Model.

4. Update Parameters:

$$\theta_t + 1 = \theta_t - \frac{\alpha \widehat{m}_t}{\sqrt{\widehat{v}_t} + \varepsilon} \tag{8}$$

During the training process, the predicted error is refined through backpropagation. Concurrently, the learning rate is progressively decreased to facilitate a more stable convergence of the model as it approaches the optimal solution.

3.3. Deep neural networks

Through a layer-by-layer abstraction and transformation within its multi-layered structure, the deep neural model learns more complex and deeper feature representations. This capability of feature learning enables the model to capture valuable information even when presented with small datasets. This deep neural network model utilizes a loss-based backpropagation algorithm to train the network for approximating a function, based on input vectors and their corresponding output vectors. Through backpropagation, the weights of the network are iteratively adjusted to optimize the mean squared error between the predicted outputs and the target outputs. The model diagram presented in this article is illustrated in Fig. 5.

The activation function used the ReLU function, the formula is:

$$f(x) = \max(0, x) \tag{9}$$

Which, $f(x)$ is the output of the ReLU activation function; x represents the input value; max (0, x) represents taking the larger value between the input value and zero.

Nadam (Nesterov-accelerated Adaptive Moment Estimation), an extension of the gradient descent optimization algorithm, is a combination of Adam (Adaptive Moment Estimation) and NAG (Nesterov Accelerated Gradient). It imposes stronger constraints on the learning rate and has a more direct influence on the update of gradients, enhancing the performance of the optimization algorithm. The formula for Nadam optimizer is:

$$\widehat{g}_t = \frac{g_t}{1 - \prod_{i=1}^{t} u_i} \tag{10}$$

$$m_t = u_t * m_{t1} + (1 - u_t) * g_t \tag{11}$$

$$m_t = \frac{m_t}{1 - \prod_{i=1}^{t+1} u_i} \tag{12}$$

$$n_t = v * n_{t1} + (1 - v) * g_t^2 \tag{13}$$

$$\widehat{n}_t = \frac{n_t}{1 - v^t} \overline{m}t = (1 - u_t) * \widehat{g}_t + u_{t+1} * \widehat{m}t \tag{14}$$

$$\triangle \theta_t = -\eta * \frac{\overline{m}_t}{\sqrt{\widehat{n}_t + e}} \tag{15}$$

The objective function, commonly referres to as the loss function, is employed to optimize the forward propagation process and minimize both expected and actual errors is:

$$LOSS = \frac{1}{n} \sum (Y_i - \widehat{Y}_i)^2 \tag{16}$$

During the training process, forward and backward propagation are conducted using small batches of data at each iteration. Forward propagation is employed to compute the model's output and assess the loss in relation to the true values. Meanwhile, backpropagation facilitates the calculation of the gradient of the loss function, enabling updates to the model parameters.

Table 3
The final optimal parameter settings.

Parameter	Value
Bootstrap	True
Max features	auto
Min samples split	2
Max depth	None
Min samples leaf	1
N estimators	100
Evaluation indicators	R^2

4. Results

In this study, the model's predictive performance was evaluated using four metrics: the coefficient of determination (R^2), mean absolute error (MAE), root mean square error (RMSE), and mean square error (MSE). These metrics quantify the accuracy and robustness of the model from different perspectives.

The coefficient of determination (R^2) measures the proportion of variance in the dependent variable that is predictable from the independent variables, a higher R^2 indicates better model fit.

$$R^2 = 1 - \frac{\sum_{i=1}^{n} (y_i - \widehat{y}_i)^2}{\sum_{i=1}^{n} (y_i - \overline{y})^2} \tag{17}$$

Mean absolute error (MAE) reflects the average magnitude of errors in a set of predictions, without considering their direction.

$$MAE = \frac{1}{n} \sum_{i=1}^{n} \left| y_i - \widehat{y}_i \right| \tag{18}$$

Root mean square error (RMSE) measures the square root of the average squared differences between predicted and actual values, penalizing larger errors more heavily.

$$RMSE = \sqrt{\frac{1}{n} \sum_{i=1}^{n} (y_i - \widehat{y}_i)^2} \tag{19}$$

Mean square error (MSE) calculates the average of the squares of the errors and is useful for identifying variance in prediction errors.

$$MSE = \frac{1}{n} \sum_{i=1}^{n} (y_i - \widehat{y}_i)^2 \tag{20}$$

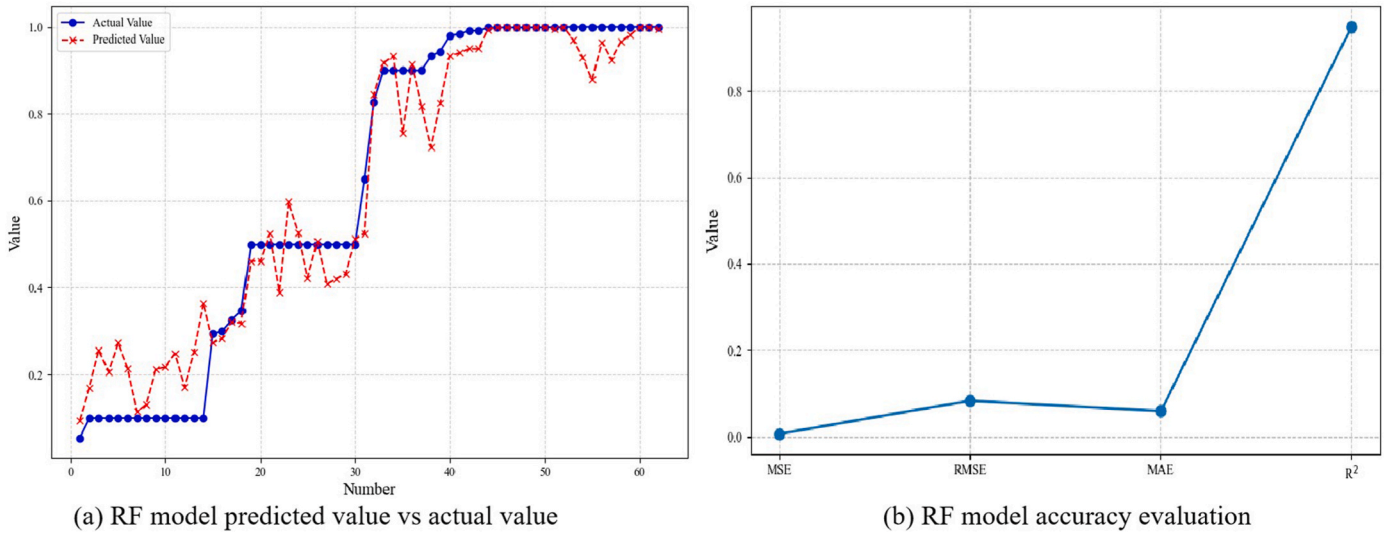

(a) RF model predicted value vs actual value (b) RF model accuracy evaluation

Fig. 6. RF model results analysis.

4.1. Random forest model

The model extracts feature values and target variables from the training dataset, employing standardization to transform the feature values into a distribution characterized by a mean of 0 and a standard deviation of 1. The incorporation of polynomial features allows the model to capture more intricate relationships. A parameter grid is established for the random forest regression model, followed by parameter tuning utilizing GridSearchCV. The model is subsequently trained with the optimal parameters, and its performance is assessed through cross-validation. The final optimal parameter settings are shown in Table 3.

Where, setting Bootstrap = True enhances model stability and reduces variance in small samples through resampling. Max features = 'auto' uses a single feature for splitting when there are only two independent variables, balancing tree diversity and overfitting risks. Min samples split = 2 and Min samples leaf = 1 allow the trees to grow fully, capturing potential patterns in the limited data. Max depth = None avoids restricting complexity, accommodating potential nonlinear relationships. N_estimators = 100 ensures sufficient ensemble performance while keeping computational costs manageable. The use of the R^2 metric for optimization indicates a focus on maximizing explained variance rather than controlling absolute errors. Overall, this parameter configuration considers model expressiveness in small-data scenarios while maintaining generalization ability through feature randomness and Bagging mechanisms.

During the model training process, the data is divided into training and testing sets with a ratio of 5:1. The comparison between the actual values and the predicted values generated by the model is illustrated in Fig. 6 (a).

As illustrated in Fig. 6 (b), the Root Mean Square Error (RMSE) is low, thus the model demonstrates strong performance in predicting probability values, with minimal discrepancies between predicted and actual values. A result of Mean Squared Error (MSE) divided by Mean Absolute Error (MAE) approaching zero indicates a higher accuracy in the model's predictions. Additionally, the R^2 as high as 95 % indicates a good fit of the model to the data.

4.2. Convolutional neural network model

This model comprises one input layer, three convolutional layers, three activation layers, one pooling layer, and two fully connected layers. The input layer scales the data to the interval [0, 1] and normalizes both the input features and target values to enhance model training stability and efficiency. The normalized data is then rearranged into a format compatible with Convolutional Neural Network (CNN) inputs, adopting a two-dimensional shape of (2, 1, 1, N). To optimize model performance, the Adam optimizer and the ReLU activation function were adopted with a training batch size of 12, a maximum iteration count of 2400, and a learning rate initialized to 0.001. After the model training is completed, the predicted results must be normalized and restored to their original size. The specific parameter settings are shown in Table 4.

Table 4
Parameter values for deep neural network models.

Parameter	Value
Pooling layer	1
First convolutional layer	512
Third convolutional layer	256
Activation function	ReLU
Iterations	2400
Fully connected layer	2
Second convolutional layer	256
Learning rate	0.001
Batch size	12

Where, pooling layer = 1 reduces feature dimensionality through a single pooling operation, avoiding excessive information compression. The convolutional layer progressively decrease from 512 to 256 to 256, extracting higher-level features while effectively controlling model complexity. The ReLU activation function provides non-linear expressive power and mitigates the vanishing gradient problem. Iterations = 2400 ensures model convergence by allowing sufficient training cycles on limited data. Fully connected layer = 2 limits the number of fully connected layers to prevent overfitting. A learning rate of 0.001 is chosen to ensure training stability. Finally, a batch size of 12 balances computational efficiency and gradient update stability for small datasets.

During the model training process, so as to meet the two-dimensional format of the convolutional neural network model, the data is divided into training and testing sets with a ratio of 5:1. The output results indicate that the R^2 between the predicted values and the true values of the training set is 94.01 %. The comparison between the predicted values and the actual values generated by the model is depicted in Fig. 7 (a). Fig. 7 (b) demonstrates the evaluation of the random forest model is conducted through four aspects, including MSE, RMSE, MAE and R^2.

As shown in Fig. 7 (b), the low RMSE value indicates that the model

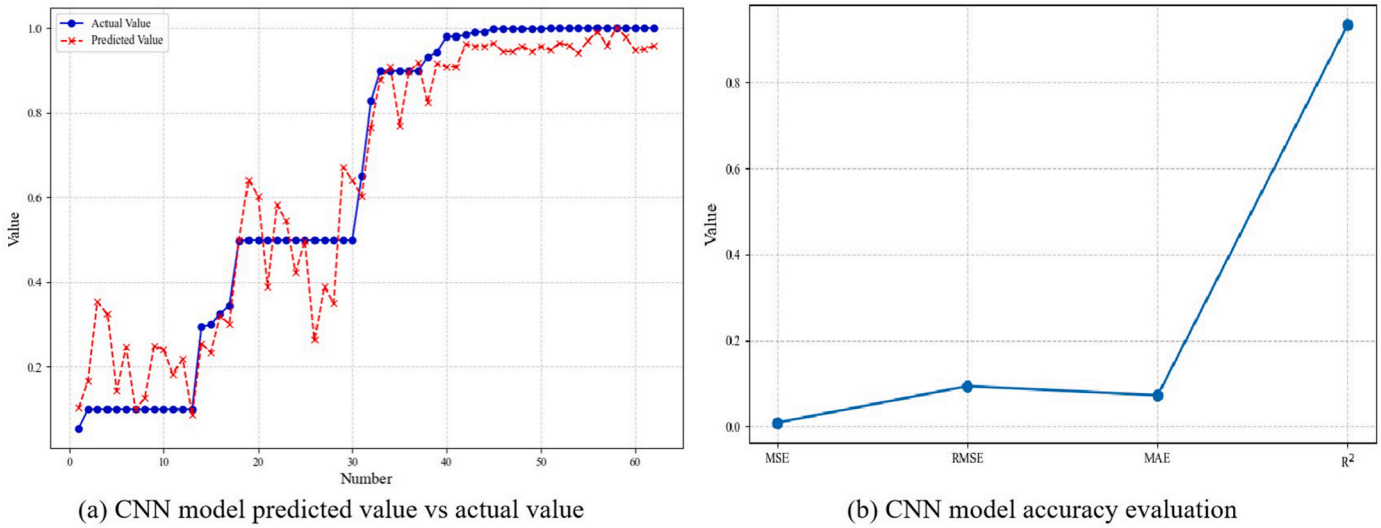

(a) CNN model predicted value vs actual value (b) CNN model accuracy evaluation

Fig. 7. CNN model results analysis.

Table 5
Parameter values for deep neural network models.

Parameter	Value
First hidden layer	256
Second hidden layer	128
Third hidden layer	96
Learning rate	0.001
Activation function	ReLU
Iterations	2000
Batch size	13

has a strong performance in predicting probability value, and the predicted value is very close to the actual value. The ratio of MAE to MSE is close to zero, indicating that the prediction accuracy of this model is high. The R^2 value is 94 %, indicating a good fit between the model and the data.

4.3. Deep neural network

In this model, an input layer, three hidden layers, and an output layer are employed. The input layer utilizes the StandardScaler function for data preprocessing to standardize the dataset effectively. Each hidden layer comprises multiple neurons, applying the ReLU activation function to perform element by element nonlinear transformations on the input data. The specific parameter settings are shown in Table 5.

Where, hidden layers (256→128→96) adopt a progressively decreasing architecture to achieve controlled feature abstraction. This hierarchical dimensionality reduction balances feature extraction capacity with model complexity, mitigating overfitting risks inherent to limited datasets. ReLU activation function introduces non-linearity to enhance representational power while alleviating the vanishing gradient problem. In small-data scenario training, the learning rate (0.001) and batch size (13) work together to stabilize gradient updates. A smaller learning rate limits parameter update steps, which avoids overshooting the optimal solution. A moderate batch size balances computational efficiency and gradient estimation reliability. Smaller batches are computationally efficient and larger batches provide more reliable gradient estimates. 2000 iterations ensure sufficient exposure of the model to the limited training data for effective parameter convergence.

During the training process of the model, the data is divided into training and testing sets with a ratio of 5:1. Among them, blue represents the true value, while red represents the predicted value. The comparison

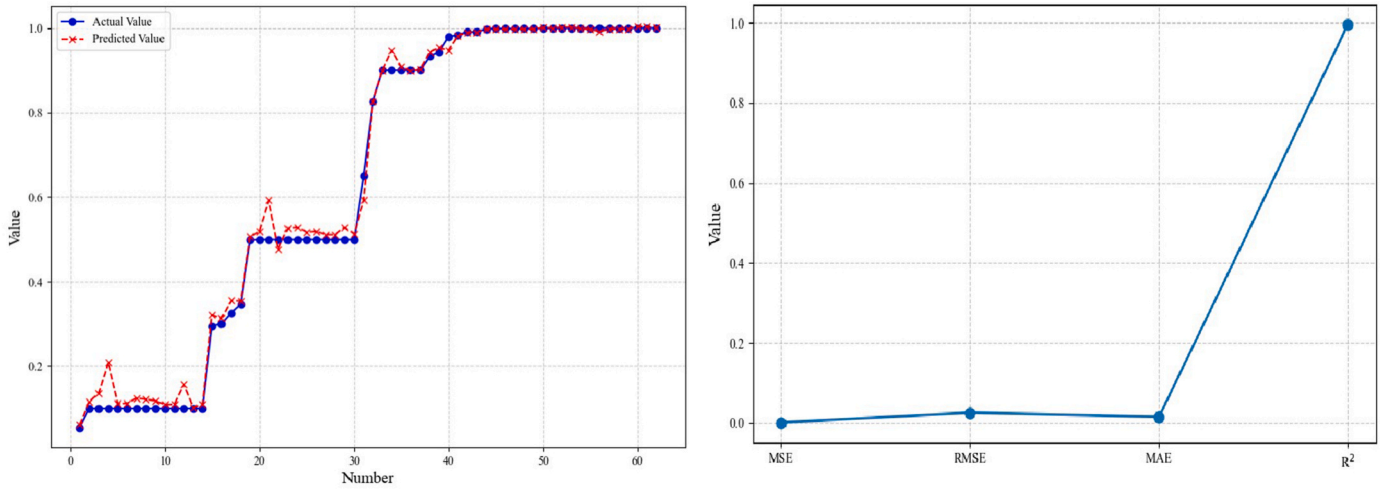

(a) DNN model predicted value vs actual value (b) DNN model accuracy evaluation

Fig. 8. DNN model results analysis.

Table 6
Summary of the accuracy (R-squared) of probability models for various process equipment.

R^2	References
0.71	Cozzani and Salzano (2004)
0.85	Zhang and Jiang (2008)
0.93	Mukhim et al. (2017a)
0.95	Present work (Random Forest Model)
0.94	Present work (Convolutional Neural Network Model)
0.99	Present work (Deep Neural Network)

between the predicted and actual values of the model is shown in Fig. 8 (a).

As illustrated in Fig. 8 (b), the root mean square error (RMSE) was recorded at 0.025, signifying that the model demonstrates robust predictive performance for probability values, with predicted outcomes closely aligning with actual observations. The ratio of mean square error (MSE) to mean absolute error (MAE) approaches zero, further indicating a high level of prediction accuracy within the model. Additionally, the R^2 value stands at 99 %, suggesting that the model exhibits an excellent fit to the data.

5. Discussion

During the model development phase, GridSearchCV was employed for hyperparameter optimization, an exhaustive search method in Scikit-learn that systematically evaluates all specified parameter combinations through cross-validation. This rigorous approach ensures the identification of optimal hyperparameter settings that maximize model performance (Devasahayam and Albijanic, 2024). While the initial grid search process can be computationally intensive due to its comprehensive exploration of the parameter space, this optimization is a one-time procedure. Once the optimal hyperparameter configuration is determined, subsequent model training eliminates the need for further parameter exploration. With the finalized parameters, the model achieves efficient training times of typically 3–5 s per session.

Table 6 compares the R^2 calculated for the literature models for equipment damage probability with respect to blast wave intensity with that obtained for the three models developed in the present study. Clearly, the machine learning-based models proposed herein show a significantly higher accuracy compared to traditional regression models. The relative error analysis of the training sets for these three models is illustrated in Fig. 9 (a). Among the three models developed in the present study, the neural network model demonstrates a superior performance.

The initial partition of the data reserved part of the data as a test set, evaluating the reliability of the training model. The R^2 of the deep neural network model reached to 93.04 %, the relative error analysis in the test set of deep neural network model is shown in Fig. 9 (b). These findings indicate that the deep neural network model developed in the present study demonstrates a strong adaptability for risk assessment of domino effects induced by overpressure in the chemical processing industry.

6. Conclusions

This paper develops a machine learning approach to improve probit models for the risk assessment of blast waves-induced domino effects in the chemical process industries. The results obtained evidence that: (i) given the characteristics of nonlinear data, fitting and solving probability values using linear regression equations raises significant challenges; (ii) three machine learning models are utilized to predict the probability values triggered by blast waves, achieving prediction accuracies of 95 % for the RF Model, 94 % for the CNN Model, and 99 % for the DNN Model; (iii) the DNN exhibited a higher accuracy. The DNN model is capable of continuously adjusting its parameters through a feedforward mechanism, enabling it to increasingly align with the underlying data distribution. Furthermore, testing has confirmed that the DNN model demonstrates stability, achieving a prediction accuracy of 93.04 % on the test set; (iv) as accident data continues to accumulate (such as critical dynamic parameters of fragment projection), this model will have access to an expanding dataset for training purposes, thereby further enhancing its predictive accuracy; (v) the models developed may also be integrated into quantitative approaches for domino risk assessment to improve domino effect prevention and management.

CRediT authorship contribution statement

Min Jiang: Writing – original draft, Methodology, Data curation. **Yu Yang:** Writing – review & editing, Resources. **Jiexiang Bian:** Writing – review & editing, Investigation. **Mengru Fang:** Writing – review & editing, Investigation. **Valerio Cozzani:** Writing – review & editing, Investigation. **Genserik Reniers:** Writing – review & editing, Investigation. **Chao Chen:** Writing – review & editing, Supervision, Conceptualization.

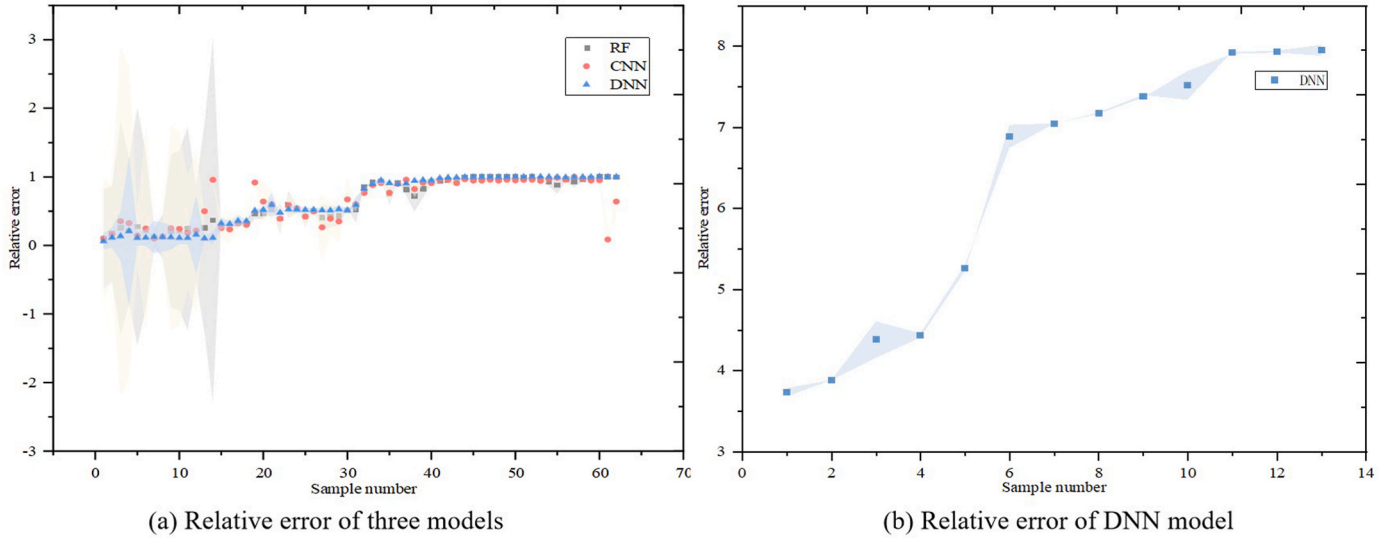

Fig. 9. Relative error chart.

Declaration of competing interest

The authors declare that they have no known competing for financial interests or personal relationships that could have appeared to influence the work reported in this paper.

Acknowledgements

This study was supported by the Sichuan Province Science and Technology Support Program (Grant No. 2025YFHZ0176 and 2023YFS0412).

Data availability

Data will be made available on request.

References

Alileche, N., Cozzani, V., Reniers, G., Estel, L., 2015. Thresholds for domino effects and safety distances in the process industry: a review of approaches and regulations. Reliab. Eng. Syst. Saf. 143, 74–84. https://doi.org/10.1016/j.ress.2015.04.007.

Biau, G., Scornet, E., 2016. A random forest guided tour. Test 25, 197–227. https://link.springer.com/article/10.1007/s11749-016-0481-7.

Casciano, M., Khakzad, N., Reniers, G., Cozzani, V., 2019. Ranking chemical industrial clusters with respect to safety and security using analytic network process. Process Saf. Environ. Prot. 132, 200–213. https://doi.org/10.1016/j.psep.2019.10.024.

CBS, 2015. Final investigation report CARIBBEAN petroleum tank terminal explosion and multiple tank fires. https://www.csb.gov/caribbean-petroleum-refining-tank-explosion-and-fire/.

CCPS, 1999. Guidelines for Chemical Process Quantitative Risk Analysis, second ed. John Wiley & Sons, Inc., New York.

Chen, C., Reniers, G., Zhang, L., 2018. An innovative methodology for quickly modeling the spatial-temporal evolution of domino accidents triggered by fire. J. Loss Prev. Process. Ind. 54, 312–324. https://doi.org/10.1016/j.jlp.2018.04.012.

Cho, J., Kim, H., Gebreselassie, A., Shin, D., 2018. Deep neural network and random forest classifier for source tracking of chemical leaks using fence monitoring data. J. Loss Prev. Process. Ind. 56, 548–558. https://doi.org/10.1016/j.jlp.2018.01.011.

Cozzani, V., Gubinelli, G., Antonioni, G., Spadoni, G., Zanelli, S., 2005. The assessment of risk caused by domino effect in quantitative area risk analysis. J. Hazard Mater. 127, 14–30. https://doi.org/10.1016/j.jhazmat.2005.07.003.

Cozzani, V., Gubinelli, G., Salzano, E., 2006. Escalation thresholds in the assessment of domino accidental events. J. Hazard Mater. 129, 1–21. https://doi.org/10.1016/j.jhazmat.2005.08.012.

Cozzani, V., Reniers, G., 2021. Dynamic Risk Assessment and Management of Domino Effects and Cascading Events in the Process Industry. Elesvier, USA.

Cozzani, V., Salzano, E., 2004. The quantitative assessment of domino effects caused by overpressure. J. Hazard Mater. 107, 67–80. https://doi.org/10.1016/j.jhazmat.2003.09.013.

Devasahayam, S., Albijanic, B., 2024. Predicting hydrogen production from co-gasification of biomass and plastics using tree based machine learning algorithms. Renew. Energy 222, 119883. https://doi.org/10.1016/j.renene.2023.119883.

Eisenberg, N., Lynch, C., Breeding, R., 1975. Vulnerability Model. A Simulation System for Assessing Damage Resulting from Marine Spills. Enviro Control Inc., USA.

Esteva, A., Kuprel, B., Novoa, R., Ko, J., Swetter, S., Blau, H., Thrun, S., 2017. Dermatologist-level classification of skin cancer with deep neural networks. Nature 542, 115–118. https://www.nature.com/articles/nature21056.

Hamid, A., Hasan, A.H., Azhari, S.N., Harun, Z., Putra, Z.A., 2022. Hybrid modelling for remote process monitoring and optimisation. Digital Chemical Engineering 4, 100044. https://doi.org/10.1016/j.dche.2022.100044.

Hassan, O., Khan, Z., Irfan, M., Rashid, M., 2025. Beyond ALOHA-quickly predict accidental release of toxic chemicals using machine learning. J. Loss Prev. Process. Ind. 94, 105542. https://doi.org/10.1016/j.jlp.2024.105542.

Jablonka, K., Charalambous, C., Sanchez Fernandez, E., Wiechers, G., Monteiro, J., Moser, P., Smit, B., Garcia, S., 2023. Machine learning for industrial processes forecasting amine emissions from a carbon capture plant. Sci. Adv. 9, 1–11. https://www.science.org/doi/full/10.1126/sciadv.adc9576.

Khan, F., Abbasi, S., 2001. An assessment of the likelihood of occurrence,and the damage potential of domino effect (chain of accidents) in a typical cluster of industries. J. Loss Prev. Process. Ind. 14, 283–306. https://doi.org/10.1016/S0950-4230(00)00048-6.

Lan, M., Gardoni, P., Qin, R., Zhang, X., Zhu, J., Lo, S., 2022. Modeling NaTech-related domino effects in process clusters: a network-based approach. Reliab. Eng. Syst. Saf. 221. https://doi.org/10.1016/j.ress.2022.108329.

Landucci, G., Gubinelli, G., Antonioni, G., Cozzani, V., 2009. The assessment of the damage probability of storage tanks in domino events triggered by fire. Accid. Anal. Prev. 41, 1206–1215. https://doi.org/10.1016/j.aap.2008.05.006.

Li, H., Jiao, J., Liu, Z., Lin, J., Zhang, T., Liu, H., 2025. Trustworthy Bayesian deep learning framework for uncertainty quantification and confidence calibration: application in machinery fault diagnosis. Reliab. Eng. Syst. Saf. 255, 110657. https://doi.org/10.1016/j.ress.2024.110657.

Malik, A., Nasif, M., Arshad, U., Mokhtar, A., Tohir, M., Al-Waked, R., 2023. Predictive modelling of wind-influenced dynamic fire spread probability in tank farm due to domino effect by integrating numerical simulation with ANN. Fire 6. https://doi.org/10.3390/fire6030085.

Men, J., Ji, H., Chen, Z., Xie, W., Zhang, L., 2021. Study of the situation deduction of a domino accident caused by overpressure in LPG storage tank area. J. Loss Prev. Process. Ind. 72, 104525. https://doi.org/10.1016/j.jlp.2021.104525.

Meng, H., Hu, M., Kong, Z., Niu, Y., Liang, J., Nie, Z., Xing, J., 2024. Risk analysis of lithium-ion battery accidents based on physics-informed data-driven Bayesian networks. Reliab. Eng. Syst. Saf. 251, 110294. https://doi.org/10.1016/j.ress.2024.110294.

Meng, H., Zhao, S., Song, W., Hu, M., 2025. Virtual-reality-generated-data-driven Bayesian networks for risk analysis. Reliab. Eng. Syst. Saf. 260, 111053. https://doi.org/10.1016/j.ress.2025.111053.

Mukhim, E., Abbasi, T., Tauseef, S., Abbasi, S., 2017a. Domino effect in chemical process industries triggered by overpressure—Formulation of equipment-specific probits. Process Saf. Environ. Prot. 106, 263–273. https://doi.org/10.1016/j.psep.2017.01.004.

Mukhim, E., Abbasi, T., Tauseef, S., Abbasi, S., 2017b. Domino effect in chemical process industries triggered by overpressure—Formulation of equipment-specific probits. Process Saf. Environ. Prot. 106, 263–273. https://doi.org/10.1016/j.psep.2017.01.004.

Nie, Z., Gao, W., Jiang, H., Lu, J., Lu, Z., Jiang, X., 2024. Predicting critical flame quenching thickness using machine learning approach with ResNet and ANN. J. Loss Prev. Process. Ind. 92, 105448. https://doi.org/10.1016/j.jlp.2024.105448.

Pourkeramat, A., Daneshmehr, A., Jalili, S., Aminfar, K., 2021. Investigation of wind and smoke concentration effects on thermal instability of cylindrical tanks with fixed roof subjected to an adjacent fire. Thin-Walled Struct. 160. https://doi.org/10.1016/j.tws.2020.107384.

Reniers, G., Cozzani, V., 2013a. Domino Effects in the Process Industries: Modeling, Prevention and Managing. Elsevier Science & Technology Books, USA.

Reniers, G., Cozzani, V., 2013b. Domino Effects in the Process Industries: Modeling, Prevention and Managing. Newnes, USA.

Reniers, G.L.L., Dullaert, W., Ale, B.J.M., Soudan, K., 2005. The use of current risk analysis tools evaluated towards preventing external domino accidents. J. Loss Prev. Process. Ind. 18, 119–126. https://doi.org/10.1016/j.jlp.2005.03.001.

Roxas II, R., Evangelista, M.A., Sombillo, J.A., Nnabuife, S.G., Pilario, K.E., 2022. Machine learning based flow regime identification using ultrasonic doppler data and feature relevance determination. Digital Chemical Engineering 3, 100024. https://doi.org/10.1016/j.dche.2022.100024.

Salzano, E., Cozzani, V., 2004a. The Use of Probit Functions in the Quantitative Risk Assessment of Domino Accidents Caused by Overpressure. Springer, London.

Salzano, E., Cozzani, V., 2004b. The Use of Probit Functions in the Quantitative Risk Assessment of Domino Accidents Caused by Overpressure. Springer, London.

Tian, Y., Guan, X., Sun, H., Bao, Y., 2024. An adaptive structural dominant failure modes searching method based on graph neural network. Reliab. Eng. Syst. Saf. 243. https://doi.org/10.1016/j.ress.2023.109841.

Wang, J., Guo, Q., Wang, F., Aviso, K., Tan, R., Jia, X., 2021. System dynamics simulation for park-wide environmental pollution liability insurance. Resour. Conserv. Recycl. 170, 105578. https://doi.org/10.1016/j.resconrec.2021.105578.

Wang, C., Zhao, Y., Addai, E., 2017. Investigation on propagation mechanism of large scale mine gas explosions. J. Loss Prev. Process. Ind. 49, 342–347. https://doi.org/10.1016/j.jlp.2017.07.011.

Xing, L., Gardoni, P., Zhou, Y., Zhang, P., 2025. DNN-metamodeling and fragility estimate of high-rise buildings with outrigger systems subject to seismic loads. Reliab. Eng. Syst. Saf. 253. https://doi.org/10.1016/j.ress.2024.110572.

Xinhua, 2023a. 9 dead, 1 injured, 1 missing in east China chemical plant explosion. http://en.people.cn/n3/2023/0504/c90000-20013786.html.

Xinhua, 2023b. 24 workers injured in blaze at chemical plant in India's Gujarat. http://en.people.cn/n3/2023/1129/c90000-20103949.html.

Xinhua, 2024. 5 killed, 14 injured in industrial park blast in China's Henan. http://en.people.cn/n3/2024/0727/c90000-20198891.html.

Yang, J., Zhang, M., Zuo, Y., Cui, X., Liang, C., 2023. Improved models of failure time for atmospheric tanks under the coupling effect of multiple pool fires. J. Loss Prev. Process. Ind. 81, 104957. https://doi.org/10.1016/j.jlp.2022.104957.

Yang, X., Li, Y., Chen, Y., Li, Y., Dai, L., Feng, R., Duh, Y.-S., 2020. Case study on the catastrophic explosion of a chemical plant for production of m-phenylenediamine. J. Loss Prev. Process. Ind. 67, 104232. https://doi.org/10.1016/j.jlp.2020.104232.

Zeng, T., Wei, L., Reniers, G., Chen, G., 2024. A comprehensive study for probability prediction of domino effects considering synergistic effects. Reliab. Eng. Syst. Saf. 251, 110318. https://doi.org/10.1016/j.ress.2024.110318.

Zhang, M., Jiang, J., 2008. An improved probit method for assessment of domino effect to chemical process equipment caused by overpressure. J. Hazard Mater. 158, 280–286. https://doi.org/10.1016/j.jhazmat.2008.01.076.

Zhang, N., Shen, S., Zhou, A., Chen, J., 2019. A brief report on the March 21, 2019 explosions at a chemical factory in Xiangshui, China. Process Saf. Prog. 38. https://doi.org/10.1002/prs.12060.

Zhang, X., Wang, Q., Bi, X., Li, D., Liu, D., Yu, Y., Tse, C.K., 2024. Mitigating cascading failure in power grids with deep reinforcement learning-based remedial actions. Reliab. Eng. Syst. Saf. 250, 110242. https://doi.org/10.1016/j.ress.2024.110242.

Zhao, H., Chen, Z., Shu, X., Xiao, R., Shen, J., Liu, Y., Liu, Y., 2024. Online surface temperature prediction and abnormal diagnosis of lithium-ion batteries based on hybrid neural network and fault threshold optimization. Reliab. Eng. Syst. Saf. 243, 109798. https://doi.org/10.1016/j.ress.2023.109798.

Zhu, J., Sun, W., Li, S., Yao, K., Song, J., 2024. Threshold-based earthquake early warning for high-speed railways using deep learning. Reliab. Eng. Syst. Saf. 250, 110268. https://doi.org/10.1016/j.ress.2024.110268.